MATERIAL SCIENCE / МАТЕРИАЛОВЕДЕНИЕ

UDC 621:538.911:538.951
DOI 10.17073/0368-0797-2023-2-197-205

Original article
Оригинальная статья

Electron beam additive manufacturing of composite alloy from stainless steel and aluminum bronze: Microstructure and mechanical properties

A. P. Zykova, A. O. Panfilov, A. V. Chumaevskii, A. V. Vorontsov, S. Yu. Tarasov

Institute of Strength Physics and Materials Science, Siberian Branch of the Russian Academy of Sciences (2/4 Akademicheskii Ave., Tomsk 634055, Russian Federation)

zykovaap@mail.ru

Abstract. The authors investigated the microstructure, phase composition and mechanical properties of the steel-bronze composite obtained by electron beam additive manufacturing with simultaneous supply of aluminum bronze wires BrAMc9-2 and stainless steel 06Kh18N9T. *X*-ray diffraction analysis revealed that the composite contains 25 % (vol.) of aluminum bronze, which leads to the formation of a three-phase structure consisting of γ-Fe, α-Fe and α-Cu grains. According to scanning electron microscopy, the volume fraction of austenite, ferrite and bronze in the steel – 25 % bronze composite is 40.7, 35.7 and 23.6 %, respectively. Unstable conditions of the electron beam additive manufacturing process lead to the release of dispersed particles in austenite and ferrite grains. Dispersion-hardened copper particles with an average particle size of 40 nm, the volume fraction of which is 47 %, are isolated in austenite grains. Dispersion-hardened NiAl particles with a volume fraction of 20 % are isolated in ferrite grains, the average size of which is 44 nm. Transmission electron microscopy data indicate the coherent conjugation of arrays of dispersion-hardened particles with the matrix. Such a composite structure provides an increase in yield strength and tensile strength by an average of 400 and 600 MPa compared with yield strength and tensile strength of 06Kh18N9T steel obtained by electron beam additive manufacturing without bronze addition. Microhardness of the composite is on average 2.2 GPa, which is 0.4 GPa higher than that of 06Kh18N9T steel obtained by electron beam additive manufacturing without bronze addition.

Keywords: electron beam additive technology, two-wire additive manufacturing, aluminum bronze, austenitic steel, steel – bronze composite, microstructure, mechanical properties

Acknowledgements: The work was supported by the grant No. NSh-1174.2022.4 of the President of the Russian Federation for state support of leading scientific schools. The work was also performed within the framework of the state task of the Institute of Strength Physics and Materials Science, Siberian Branch of the Russian Academy of Sciences, projects FWRW-2021-0012. The research was carried out using the equipment of the Research Center "Nanotech" of the Institute of Strength Physics and Materials Science, Siberian Branch of the Russian Academy of Sciences.
The authors express their gratitude to Professor A.I. Lotkov for valuable comments on the article.

For citation: Zykova A.P., Panfilov A.O., Chumaevskii A.V., Vorontsov A.V., Tarasov S.Yu. Electron beam additive manufacturing of composite alloy from stainless steel and aluminum bronze: Microstructure and mechanical properties. *Izvestiya. Ferrous Metallurgy*. 2023;66(2):197–205. https://doi.org/10.17073/0368-0797-2023-2-197-205

Электронно-лучевое аддитивное производство композиционного сплава из нержавеющей стали и алюминиевой бронзы: микроструктура и механические характеристики

А. П. Зыкова, А. О. Панфилов, А. В. Чумаевский, А. В. Воронцов, С. Ю. Тарасов

Институт физики прочности и материаловедения Сибирского отделения РАН (Россия, 634055, Томск, пр. Академический 2/4)

zykovaap@mail.ru

Аннотация. Исследованы микроструктура, фазовый состав и механические характеристики композита сталь – бронза, полученного методом электронно-лучевого аддитивного производства с одновременной подачей проволок алюминиевой бронзы БрАМц9-2 и нержавеющей стали 06Х18Н9Т. Методом рентгеноструктурного анализа установлено, что композит содержит 25 % (об.) алюминиевой бронзы и это приводит к формированию трехфазной структуры, состоящей из зерен γ-Fe, α-Fe и α-Cu. По данным сканирующей электронной микроскопии объемная доля аустенита, феррита и бронзы в композите сталь – 25 % бронзы составляет 40,7, 35,7 и 23,6 % соответственно. Неравновесные условия процесса электронно-лучевого аддитивного производства приводят к выделению дисперсных частиц в зернах аустенита и феррита. В зернах аустенита выделяются дисперсионно упрочняемые частицы меди со средним размером частиц 40 нм, объемная доля которых составляет 47 %. В зернах феррита выделяются дисперсионно упрочняемые частицы NiAl с объемной долей 20 %, средний размер которых составляет 44 нм. Данные просвечивающей электронной микроскопии свидетельствуют о когерентном сопряжении решеток дисперсионно упрочняемых частиц с матрицей. Такая структура композита обеспечивает повышение предела текучести и предела прочности в среднем на 400 и 600 МПа по сравнению с пределом текучести и пределом прочности стали 06Х18Н9Т, полученной электронно-лучевым аддитивным производством без добавления бронзы. Микротвердость композита в среднем составляет 2,2 ГПа, что на 0,4 ГПа выше, чем у стали 06Х18Н9Т, полученной электронно-лучевым аддитивным производством без добавления бронзы.

Ключевые слова: электронно-лучевая аддитивная технология, двухпроволочное аддитивное производство, алюминиевая бронза, аустенитная сталь, композит сталь – бронза, микроструктура, механические свойства

Благодарности: Работа выполнена в рамках гранта Президента Российской Федерации для государственной поддержки ведущих научных школ НШ-1174.2022.4 и государственного задания Института физики прочности и материаловедения Сибирского отделения РАН, проект FWRW-2021-0012. Исследования выполнены с использованием оборудования ЦКП «Нанотех» Института физики прочности и материаловедения Сибирского отделения РАН.
Авторы выражают благодарность профессору А.И. Лоткову за ценные замечания, которые помогли улучшить статью.

Для цитирования: Зыкова А.П., Панфилов А.О., Чумаевский А.В., Воронцов А.В., Тарасов С.Ю. Электронно-лучевое аддитивное производство композиционного сплава из нержавеющей стали и алюминиевой бронзы: микроструктура и механические характеристики. *Известия вузов. Черная металлургия*. 2023;66(2):197–205. https://doi.org/10.17073/0368-0797-2023-2-197-205

Introduction

Electron beam additive manufacturing (EBAM) is a highly efficient and productive method of additive manufacturing (AM) [1 – 3]. This process utilizes metal wire as its source material, which is fed to the focal spot of an electron beam. Upon melting the wire, its drop is transferred into a molten pool formed in a substrate, which then solidifies to form a bead [4]. Unlike the powder-bed AM methods, EBAM may not be suitable for manufacturing complex geometries with small features (up to 1 mm), but it offers several other advantages, such as producing defect-free, high-quality items, that are difficult to obtain with the powder-bed technologies [5; 6]. Furthermore, EBAM is performed under vacuum conditions, which prevent the ingress of inclusions and oxidation, and also eliminate gas porosity in the resulting materials [7 – 9].

Austenitic stainless steel is widely used in various industries, including chemical processes, mechanical engineering, high-temperature bolt fabrication, and nuclear reactors, due to its excellent corrosion resistance, high-temperature mechanical properties, and good manufacturability and weldability. However, the production of complex geometry items with traditional manufacturing methods is both costly and labor-consuming process. The development of AM can significantly simplify the manufacturing of complex geometry items, reduce the production cost, and have a positive impact on the development of various industries. Nevertheless, the wide application of AM is limited by certain challenges, such as occurrence of high-temperature gradients and low cooling rates during the process, which can lead to formation of heterogeneous structure and phase composition [10 – 12]. For instance, an anisotropic structure and mechanical properties of stainless steel items manufactured by selective laser melting are attributed to the high ratio of the molten pool width to the layer thickness [10 – 12], and the presence of unmelted powder particles [13 – 15]. However, these defects can be avoided using direct laser sintering of powdered stainless steel, followed by impregnation with bronze [16; 17]. This technology serves not only to reduce porosity and increase the density of samples, but also to enhance the yields stress and ultimate strength of the items.

The wire-feed EBAM is effective for avoiding the gas porosity. However, there are low cooling rates that can facilitate formation of high aspect ratio columnar grains. Moreover, during the primary crystallization of columnar grains, δ-ferrite grains may form in the interdendritic spaces, which reduce the corrosion resistance of stainless steels [6; 7; 9]. Mechanical properties can be improved either by eliminating the columnar grains or refining them using ultrasonic treatment during EBAM [18]. Such a combined technology can reduce the δ-ferrite content by up to 2 %.

The metallurgical processes involved in either powder-bed or wire-feed AM differ significantly, leading to questions about the structural formation of composites when stainless steel and aluminum bronze are directly added to the molten pool. This study aims to investigate the structural phase state and mechanical properties of a steel-bronze composite produced by electron beam

additive manufacturing with simultaneous feeding of two wires.

Experimental

Workpieces of steel – 25 % bronze composite measuring 80×120×8 mm were manufactured using EBAM. The raw materials used were ⌀1.6 mm wires made of stainless steel ER321 and aluminum bronze grade CuAl9Mn2. A stainless steel plate with a thickness of 10 mm was used as the substrate. The manufacturing process is illustrated in Fig. 1, which shows the EBAM facility equipped with two wire feeders. The process parameters included a beam accelerating voltage of 30 kV, a beam current that varied between 77 to 44 mA during printing, and a table traveling speed of 400 mm/min. The required percentage of steel and bronze was maintained by automatically adjusting the respective ratio of wire feeding rates, with the feeding rate of ER321 and CuAl9Mn2 wires set at 1300 and 250 mm/min, respectively. Ultimately, the composite was manufactured with a volumetric ratio of stainless steel to bronze of 75:25.

Structural and phase composition analysis, as well as mechanical property evaluation, was conducted on samples cut according to the layout depicted in Fig. 1. The samples of the steel – 25 % bronze composite underwent conventional preparation, including grinding with emery paper (corundum) and polishing with diamond pastes of various grain sizes (14/10, 3/2 and 1/0). To expose microstructure elements, the polished surface of the composite was chemically etched using the following reagent: 30 ml HCl + 5 g $FeCl_3$–$6H_2O$ + 60 ml H_2O.

The microstructure and chemical composition of the samples were analyzed using a Thermo Fisher Scientific Apreo S LoVac scanning electron microscope equipped with an energy dispersion spectrometer (EDS). The average grain size was determined using the secant method [19], while the phase composition was analyzed using a DRON-7 *X*-ray diffractometer (CoK_α radiation). The microstructural features of the composite were studied using a JEOL-2100 transmission electron microscope. Vickers microhardness was measured using a Duramin 5 hardness meter under a 100 g load with a 1 mm step. Uniaxial tension tests were carried out using an UTS-110M universal testing machine with blades cut off in mutually perpendicular directions according to the layouts in Fig. 1.

Results and discussion

The XRD analysis showed the steel – 25 % bronze composite is composed of γ-Fe, α-Fe and α-Cu (Fig. 2). This allowed us to assume that a portion of austenite was transformed into ferrite as a consequence of fusion of stainless steel and aluminum bronze.

SEM BSE images revealed the presence of at least three structural components in the composite. (Fig. 3, a, *b*). Austenite was observed as light grey dendrites (Fig. 3, *b*), and its elemental composition was proportional to the that of the initial wire, but enriched additionally with up to 6 at. % Al and 8 at. % Cu (Fig. 3, *b*; Table 1, spectra *4* – *7*). The average size of γ-Fe grains is approximately 4.3 μm.

The light regions in the microstructure corresponded to copper-based solid solution, which was confirmed

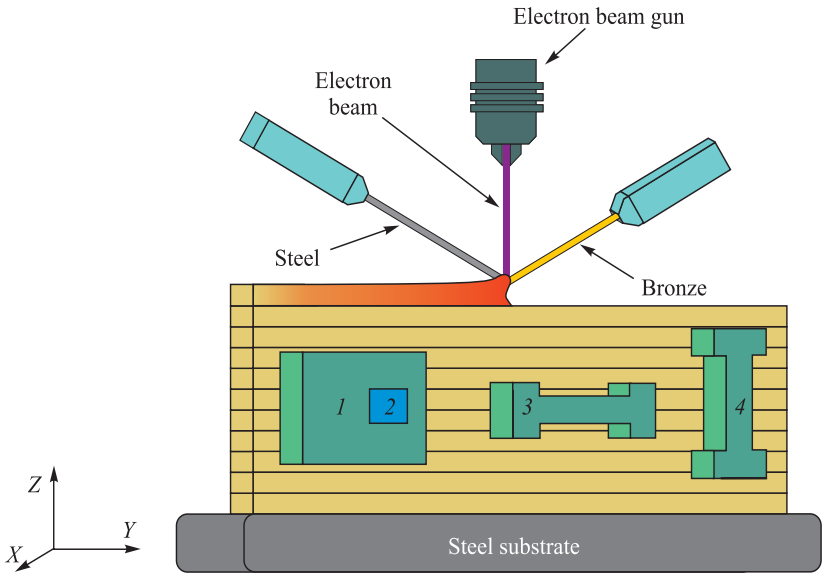

Fig. 1. Deposition path of steel – 25 % bronze composite and scheme of samples cutting for examination:
1, *2* – samples for microstructural and phase studies; *3*, *4* – samples for tensile tests

Рис. 1. Схема печати композита сталь – 25 % бронзы и схема вырезки образцов для исследований:
1, *2* – образцы для структурно-фазового исследования; *3*, *4* – образцы для испытаний на растяжение

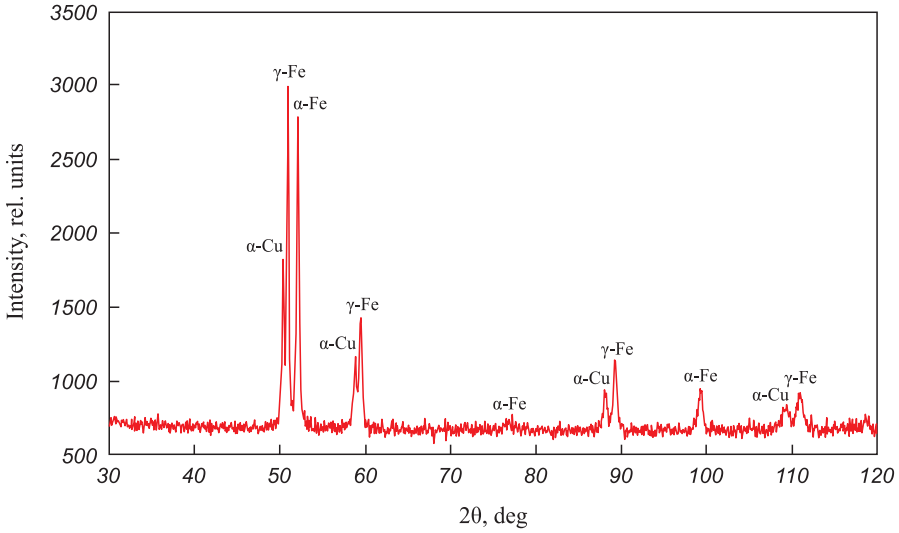

Fig. 2. XRD pattern of steel – 25 % bronze composite

Рис. 2. Рентгенограмма композита сталь – 25 % бронзы

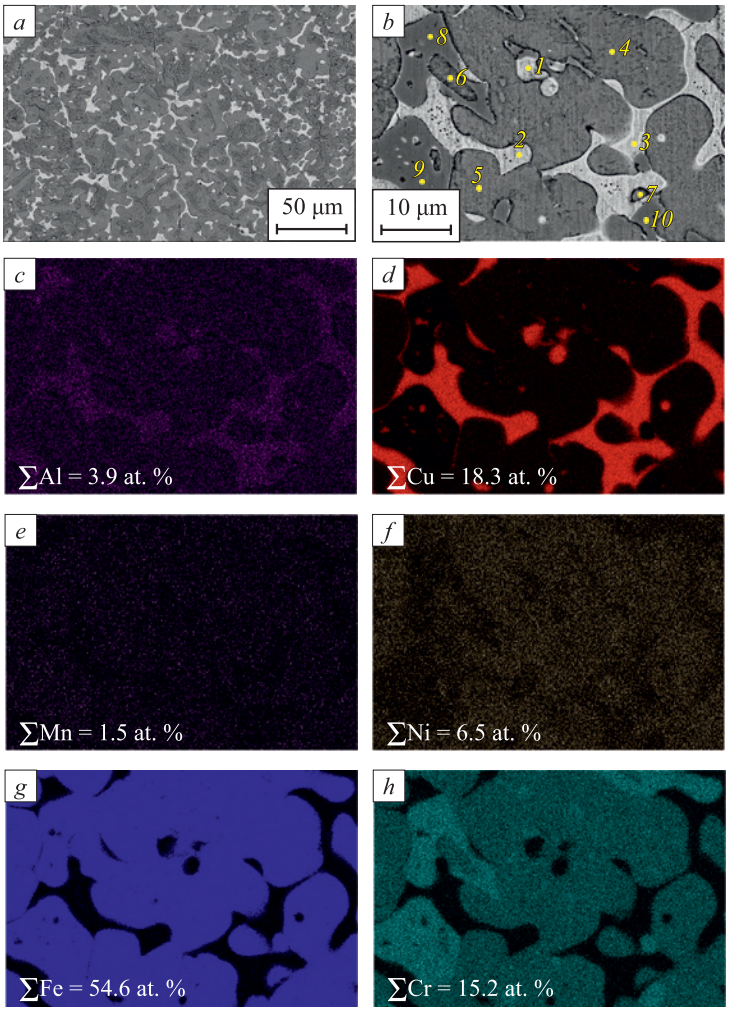

Fig. 3. SEM-BSE images (*a*, *b*), EDS element distribution maps (*f* – *h*) from section *b*: *1* – *10* – EDS spectra in selected points (Table 1)

Рис. 3. РЭМ изображения в режиме BSE (*a*, *b*); карты распределения алюминия, меди, марганца, никеля, железа, хрома (*f* – *h*), снятых с участка *b*: *1* – *10* – EDS спектры, снятые локально в указанных точках (табл. 1)

Table 1

EDS spectra of the steel – 25% bronze composite obtained by SEM

Таблица 1. **Данные EDS анализа композита сталь – 25 % бронзы**

Spectrum	Element content, at. %								Assumed phase
	Al	Si	Ti	Cr	Mn	Fe	Ni	Cu	
1	8.7	0.2	0.5	2.1	1.6	6.2	5.1	75.6	α-Cu
2	9.6	0.5	0.4	1.7	1.6	5.5	4.7	76.0	α-Cu
3	9.0	0.3	0.5	1.7	1.6	5.5	4.4	77.1	α-Cu
4	3.2	0.5	0.8	16.1	1.4	62.2	8.2	7.6	γ-Fe
5	3.2	0.6	0.7	16.1	1.4	62.8	8.2	7.0	γ-Fe
6	3.2	0.6	0.7	17.0	1.5	62.0	7.0	8.0	γ-Fe
7	5.5	0.7	0.5	13.0	1.4	64.2	6.7	8.0	γ-Fe
8	3.0	0.8	0.5	22.7	1.5	65.9	4.0	1.7	α-Fe
9	3.2	0.8	0.6	21.4	1.5	63.8	4.3	4.5	α-Fe
10	3.4	0.8	0.6	21.7	1.6	63.8	4.5	3.7	α-Fe

by the EDS element distribution maps (Fig. 3, *b*, *d*). The α-Cu based solid solution contained about 2 at. % Cr, 6 at. % Fe and 5 at. % Ni (Fig. 3, *b*; Table 1, spectra *1 – 3*), and the average size of α-Cu grains was approximately 3.1 μm.

The dark grey regions were located between α-Cu particles and corresponded to an oversaturated solid solution of chromium in α-Fe (Fig. 3, *b*). The average α-Fe grain size is 3.3 μm, and the particles belonging to ferrite were depleted with nickel to 22.7 at. %. According to SEM data, the volumetric portion of austenite, ferrite and bronze in the steel – 25 % bronze composite was 40.7, 35.7 and 23.6 %, respectively.

The element distribution maps also provide that copper particles are present in the majority of austenite grains (Fig. 3, *d*), and that nickel atoms exist in the α-Cu regions (Fig. 3, *f*). Notably, regions with higher concentration of chromium atoms are located at the periphery of austenitic grains, in the vicinity of α-Cu regions (Fig. 3, *h*), which are also depleted in nickel compared to the main background (Fig. 3, *f*). Such variations in the chromium nickel equivalent occur as a result of the dissolution of nickel atoms in α-Cu, leading to the formation of a ferrite-based solid solution.

A more detailed SEM analysis was conducted to study the microstructure of the steel – 25 % bronze composite, revealing the existence of NiAl spherical particles within the α-Fe particles (Fig. 4, *a – c*). The dark field TEM image clearly shows these NiAl particles formed at the ferrite/bronze interface (Fig. 4, *c*). EDS analysis confirmed the stoichiometric composition of NiAl particles (Fig. 4, *a*, spectrum *2*; Table 2). The average size of NiAl particles within α-Fe was found to be 44 ± 1.4 nm.

Furthermore, SAED pattern was obtained from the interlayer between grains of austenite and ferrite that revealed the existence of FCC phase with a lattice constant of $a = 3.60$ Å, corresponding to both γ-Fe and α-Cu (Fig. 4, *e*). The high copper content in the analyzed region (Fig. 4, *e*, spectrum *4*; Table 2) suggests that this is a copper-based solid solution enriched with chromium and nickel atoms. A dark field TEM image obtained in the reflection of α-Cu (Fig. 4, *f*) shows that there are

Table 2

EDS spectra of steel – 25% bronze composite obtained by TEM

Таблица 2. **Данные EDS анализа композита сталь – 25 % бронзы**

Spectrum	Element content, at. %								Assumed phase
	Al	Si	Ti	Cr	Mn	Fe	Ni	Cu	
1	5.7	1.1	1.7	20.7	0.9	57.7	6.5	5.7	α-Fe
2	41.8	–	1.3	0.8	2.1	6.9	38.3	8.7	NiAl
3	3.8	1.4	–	16.2	1.3	61.8	7.4	8.1	γ-Fe
4	10.7	–	–	0.9	1.4	3.6	5.6	77.8	α-Cu

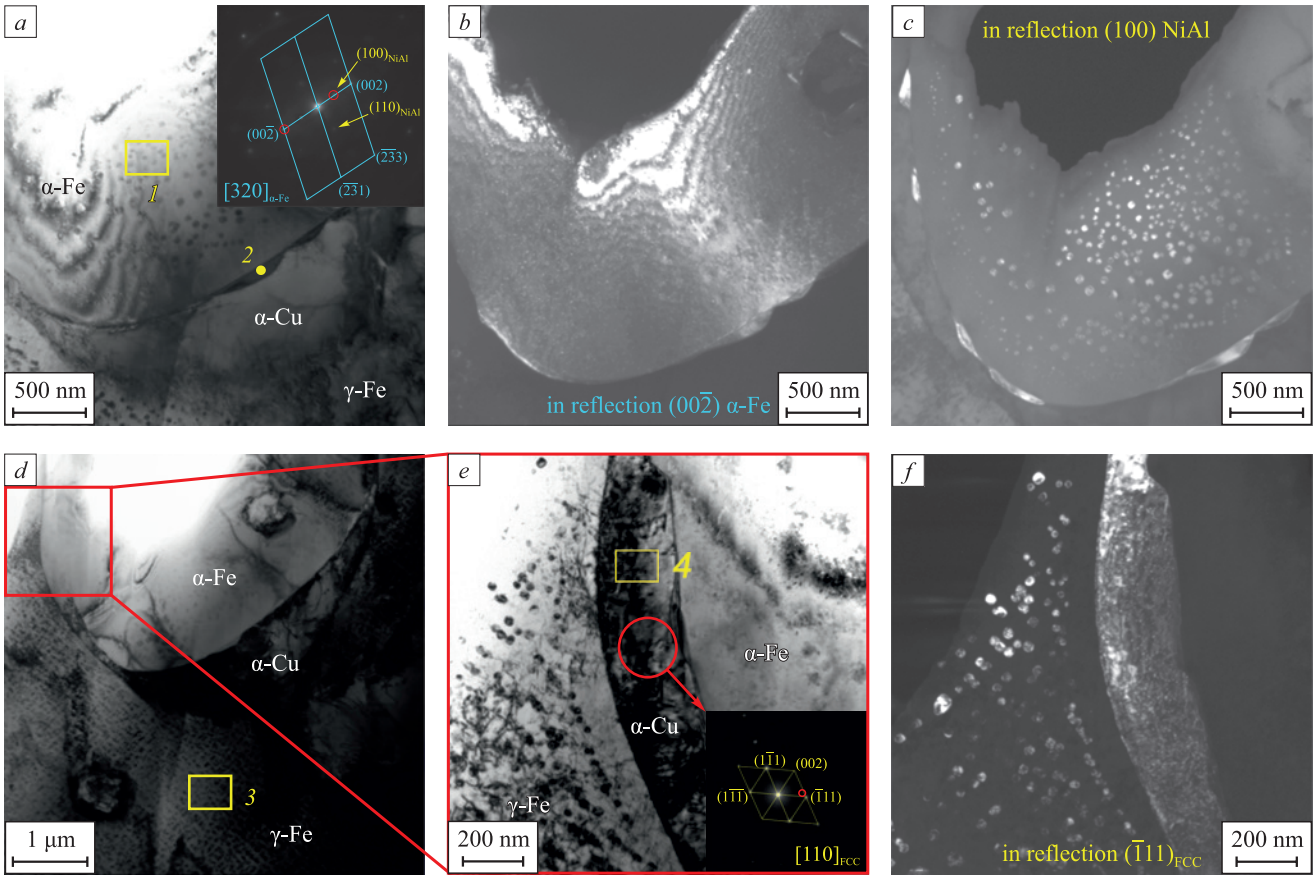

Fig. 4. TEM bright-field images of microstructures of as-deposited steel – 25 % bronze (*a*, *d*); dark-field images (*b*, *c*) obtained using $(00\bar{2})_{\alpha\text{-Fe}}$ and $(\bar{1}00)_{NiAl}$ reflections from the SAED pattern (*a*); bright-field image (*e*) of section (*d*); dark-field image (*f*) obtained using $(111)_{FCC}$

Рис. 4. Светлопольное ПЭМ-изображение фрагмента микроструктуры композита сталь – 25 % бронзы (*a*, *d*); темнопольные изображения (*b*, *c*), полученные в рефлексах $(00\bar{2})_{\alpha\text{-Fe}}$ и $(\bar{1}00)_{NiAl}$ на микродифракции с участка (*a*); светлопольное изображение (*e*) участка (*d*); темнопольное изображение (*f*) в рефлексе $(111)_{ГЦК}$

fine dispersed copper particles in γ-Fe, with an average size of about 40 ± 1.4 nm (Fig. 4, *f*). These particles may have formed in γ-Fe due to a decrease in copper solubility and precipitation of copper clusters from the oversaturated γ-Fe solid solution upon cooling.

Fig. 5 illustrates the microhardness profiles on steel grade ER321 and steel – 25 % bronze composite. The microhardness number profile of ER321 steel is stepwise, which is attributed to the presence of a sufficiently high fraction of δ-ferrite and the heterogeneities of the dendrite microstructure [18]. The microhardness of the steel – 25 % bronze composite is, on average, 2.2 ± 0.03 GPa, which is approximately 0.4 GPa higher than that of steel obtained by EBAM without addition of bronze. The higher microhardness (up to 2.9 GPa) of the steel – 25 % bronze composite is attributed to the indenter hitting into austenite grains, while the lower microhardness (down to 2 GPa) corresponds to the indenter hitting into the boundary of ferrite bronze grains (Fig. 5).

The mechanical properties of the steel – 25 % bronze composite are presented in Table 3. The yield stress and

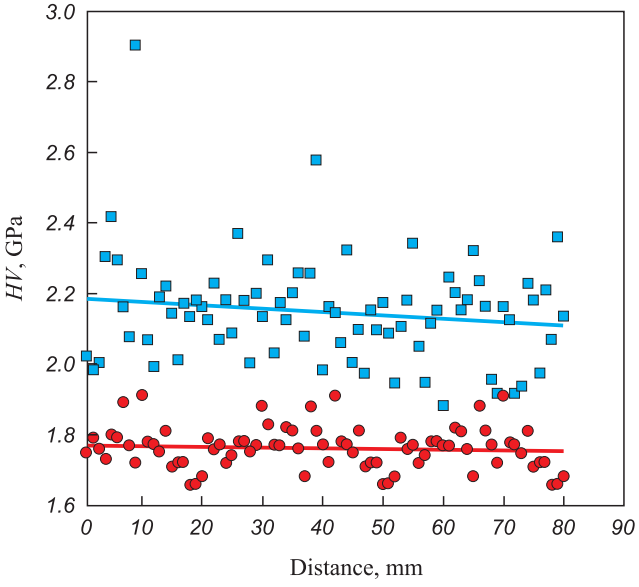

Fig. 5. Microhardness distribution profiles for steel ER321 (●) and steel – 25 % bronze composite (■)

Рис. 5. Профили распределения микротвердости стали марки 06Х18Н9Т (●) и композита сталь – 25 % бронзы (■)

Table 3

Mechanical properties of steel ER321 and steel – 25% bronze composite obtained by EBAM

Таблица 3. **Механические свойства стали марки 06Х18Н9Т и композита сталь – 25 % бронзы, полученных ЭЛАП**

Sample	$\sigma_{0.2}$, MPa	σ_u, MPa	Relative elongation, %
ER321	300 ± 15	610 ± 30	35 ± 2
steel – 25 % bronze	840 ± 42	1200 ± 57	29 ± 2

ultimate strength of the steel, grade ER321, obtained by EBAM without the addition of bronze are approximately 300 and 610 MPa, respectively (Table 3) for comparison purposes. The yield stress and ultimate strength of the steel – 25 % bronze composite increase to 840 ± 42 and 1200 ± 57 MPa, respectively. However, the relative elongation of the composite shows a minor increase compared to that of steel ER321 (Table 3).

Addition of two molten wires into the pool resulted in intermixing and mutual diffusion of both alloys' components, leading to changes in the nickel chromium equivalent and the formation of grains of α-Fe based solid solution in γ-Fe regions adjacent to α-Cu based solid solution. Additionally, the interdendrite spaces were enriched with chromium, and crystallized as δ-ferrite in cooling. Previous studies have reported such a γ → α-transformation during the manufacturing of steel – bronze composite structures using wire arc additive technology [19; 20].

Conclusions

This study investigates the microstructure and mechanical properties of a composite material produced by fusing 25 vol. % CuAl9Mn2 aluminum bronze with austenitic stainless steel using electron beam additive melting with dual wire feeding. The composite exhibits a three-phase structure, consisting of defect-free austenite, ferrite, and bronze, with the predominant phases being austenite and ferrite. Copper and NiAl particles are present, acting as dispersion hardening precipitates in the ferrite and austenite, respectively. The composite also exhibits higher microhardness (by 0.4 GPa) compared to pure steel produced via EBAM. Moreover, the yield stress and ultimate strength of the composite are increased by an average of 400 MPa and 600 MPa, respectively.

Список литературы / References

1. Stawovy M.T. Comparison of LCAC and PM Mo deposited using Sciaky EBAM™. *International Journal of Refractory Metals and Hard Materials*. 2018;73:162–167. https://doi.org/10.1016/j.ijrmhm.2018.02.009
2. Madhavadas V., Srivastava D., Chadha U., Raj S.A., Sultan M.T.H., Shahar F.S., Shah A.U.M. A review on metal additive manufacturing for intricately shaped aerospace components. *CIRP Journal of Manufacturing Science and Technology*. 2022;39:18–36. https://doi.org/10.1016/j.cirpj.2022.07.005
3. Le V.T., Paris H. Impact of total build height and batch size on environmental performance of electron beam melting. *Procedia CIRP*. 2018;69:112–117. https://doi.org/10.1016/j.procir.2017.11.013
4. Galati M. Electron beam melting process: A general overview. In: *Handbooks in Advanced Manufacturing. Chapter 8*. 2021:277–301. https://doi.org/10.1016/B978-0-12-818411-0.00014-8
5. Yin Q., Chen G., Cao H., Zhang G., Zhang B., Wei S. Transformation law of microstructure evolution and mechanical properties of electron beam freeform fabricated 321 austenitic stainless steel. *Vacuum*. 2021;194:110594. https://doi.org/10.1016/j.vacuum.2021.110594
6. Tarasov S.Yu., Filippov A.V., Shamarin N.N., Fortuna S.V., Maier G.G., Kolubaev E.A. Microstructural evolution and chemical corrosion of electron beam wire-feed additively manufactured AISI 304 stainless steel. *Journal of Alloys and Compounds*. 2019;803:364–370. https://doi.org/10.1016/j.jallcom.2019.06.246
7. Panin V.E., Narkevich N.A., Durakov V.G., Shulepov I.A. Control of the structure and wear resistance of a carbon-nitrogen austenitic steel coating produced by electron beam cladding. *Physical Mesomechanics*. 2021;24:53–60. https://doi.org/10.1134/S1029959921010082
8. Zykova A., Nikonov S., Utyaganova V., Shamarin N., Ivanov A., Chumaevskii A. Process control features of electron-beam additive manufacturing of austenitic stainless steel. *Procedia Structural Integrity*. 2020;30:216–223. https://doi.org/10.1016/j.prostr.2020.12.033
9. Wanjara P., Brochu M., Jahazi M. Electron beam freeforming of stainless steel using solid wire feed. *Materials & Design*. 2007;28(8):2278–2286. https://doi.org/10.1016/j.matdes.2006.08.008
10. Yadollahi A., Shamsaei N., Thompson S.M., Seely D.W. Effects of process time interval and heat treatment on the mechanical and microstructural properties of direct laser deposited 316L stainless steel. *Materials Science and Engineering: A*. 2015;644:171–183. https://doi.org/10.1016/j.msea.2015.07.056
11. Suryawanshi J., Prashanth K.G., Ramamurtya U. Mechanical behavior of selective laser melted 316L stainless steel. *Materials Science and Engineering: A*. 2017;696:113–121. https://doi.org/10.1016/j.msea.2017.04.058
12. Casati R., Lemke J., Vedani M. Microstructure and fracture behavior of 316L austenitic stainless steel produced by selective laser melting. *Journal of Materials Science & Technology*. 2016;32(8):738–744. https://doi.org/10.1016/j.jmst.2016.06.016
13. Narasimharaju S.R., Zeng W., See T.L., Zhu Z., Scott P., Jiang X., Lou S. A comprehensive review on laser powder bed fusion of steels: Processing, microstructure, defects and control methods, mechanical properties, current challenges and future trends. *Journal of Manufacturing Processes*. 2022;75:375–414. https://doi.org/10.1016/j.jmapro.2021.12.033

14. Leo P., D'Ostuni S., Perulli P., Sastre M.A.C., Fernández-Abia A.I., Barreiro J. Analysis of microstructure and defects in 17-4 PH stainless steel sample manufactured by Selective Laser Melting. *Procedia Manufacturing*. 2019;41:66–73. https://doi.org/10.1016/j.promfg.2019.07.030

15. Cacace S., Demir A.G., Semeraro Q. Densification mechanism for different types of stainless steel powders in Selective Laser Melting. *Procedia CIRP*. 2017;62:475–480. https://doi.org/10.1016/j.procir.2016.06.010

16. Lu S.L., Meenashisundaram G.K., Wang P., Nai S.M.L., Wei J. The combined influence of elevated pre-sintering and subsequent bronze infiltration on the microstructures and mechanical properties of 420 stainless steel additively manufactured via binder jet printing. *Additive Manufacturing*. 2020;34: 10126. https://doi.org/10.1016/j.addma.2020.101266

17. Pavankumar G., Elangovan M. Study on effect of post processing on Direct Metal LASER sintered 420 stainless steel infiltrated with bronze. *Materials Today: Proceedings*. 2018; 5(11):Part 3:24476–24485. https://doi.org/10.1016/j.matpr.2018.10.244

18. Vorontsov A., Astafurov S., Melnikov E., Moskvina V., Kolubaev E., Astafurova E. The microstructure, phase composition and tensile properties of austenitic stainless steel in a wire-feed electron beam melting combined with ultrasonic vibration. *Materials Science and Engineering: A*. 2021;820: 141519. https://doi.org/10.1016/j.msea.2021.141519

19. Gol'dshtein M.I., Litvinov V.S., Bronfin B.M. *Metallophysics of High-Strength Alloys*. Moscow: Metallurgiya; 1986: 312. (In Russ.).

Гольдштейн М.И., Литвинов В.С., Бронфин Б.М. *Металлофизика высокопрочных сплавов*. Москва: Металлургия; 1986:312.

20. Kucita P., Wang S.C., Li W.S., Cook R.B., Starink M.J. The effects of substrate dilution on the microstructure and wear resistance of PTA Cu–Al–Fe aluminium bronze coatings. *Wear*. 2019;440–441:203102. https://doi.org/10.1016/j.wear.2019.203102

21. Tao X.P., Zhang S., Zhang C.H., Wu C.L., Chen J., Abdullah A.O. Effect of Fe and Ni contents on microstructure and wear resistance of aluminum bronze coatings on 316 stainless steel by laser cladding. *Surface and Coatings Technology*. 2018;342:76–84. https://doi.org/10.1016/j.surfcoat.2018.02.032

Information about the Authors / Сведения об авторах

Anna P. Zykova, *Cand. Sci. (Phys.-Math.), Senior Researcher, Head of the Laboratory of Structural Design of Advanced Materials,* Institute of Strength Physics and Materials Science, Siberian Branch of Russian Academy of Sciences
ORCID: 0000-0001-8779-3784
E-mail: zykovaap@mail.ru

Aleksandr O. Panfilov, *Postgraduate, Junior Researcher of the Laboratory of Structural Design of Advanced Materials,* Institute of Strength Physics and Materials Science, Siberian Branch of Russian Academy of Sciences
ORCID: 0000-0001-8648-0743
E-mail: alexpl@ispms.ru

Andrei V. Chumaevskii, *Cand. Sci. (Eng.), Senior Researcher of the Laboratory of Local Metallurgy in Additive Technologies,* Institute of Strength Physics and Materials Science, Siberian Branch of Russian Academy of Sciences
ORCID: 0000-0002-1983-4385
E-mail: tch7av@gmail.com

Andrei V. Vorontsov, *Cand. Sci. (Eng.), Research Associate of the Laboratory of Local Metallurgy in Additive Technologies,* Institute of Strength Physics and Materials Science, Siberian Branch of Russian Academy of Sciences
ORCID: 0000-0002-4334-7616
E-mail: vav@ispms.ru

Sergei Yu. Tarasov, *Dr. Sci. (Eng.), Chief Researcher of the Laboratory of Physics of Surface Hardening,* Institute of Strength Physics and Materials Science, Siberian Branch Russian Academy of Sciences
ORCID: 0000-0003-0702-7639
E-mail: tsy@ispms.ru

Анна Петровна Зыкова, *к.ф.-м.н., старший научный сотрудник, заведующий лабораторией структурного дизайна перспективных материалов,* Институт физики прочности и материаловедения СО РАН
ORCID: 0000-0001-8779-3784
E-mail: zykovaap@mail.ru

Александр Олегович Панфилов, *аспирант, младший научный сотрудник лаборатории структурного дизайна перспективных материалов,* Институт физики прочности и материаловедения СО РАН
ORCID: 0000-0001-8648-0743
E-mail: alexpl@ispms.ru

Андрей Валерьевич Чумаевский, *к.т.н., старший научный сотрудник лаборатории локальной металлургии в аддитивных технологиях,* Институт физики прочности и материаловедения СО РАН
ORCID: 0000-0002-1983-4385
E-mail: tch7av@gmail.com

Андрей Владимирович Воронцов, *к.т.н., научный сотрудник лаборатории локальной металлургии в аддитивных технологиях,* Институт физики прочности и материаловедения СО РАН
ORCID: 0000-0002-4334-7616
E-mail: vav@ispms.ru

Сергей Юльевич Тарасов, *д.т.н., главный научный сотрудник лаборатории физики упрочнения поверхности,* Институт физики прочности и материаловедения СО РАН
ORCID: 0000-0003-0702-7639
E-mail: tsy@ispms.ru

Contribution of the Authors / Вклад авторов

A. P. Zykova – formation of the main article concept, preparation of illustrations, interpretation and analysis of data by transmission electron microscopy, calculation of contributions of individual hardening mechanisms.

А. П. Зыкова – формирование основной концепции статьи, подбор иллюстраций, расшифровка и анализ данных методом просвечивающей электронной микроскопии, описание результатов.

A. O. Panfilov – investigation of microstructure by optical microscopy, analysis of the results of microstructural studies, performing mechanical tensile tests.

A. V. Chumaevskii – investigation of microstructure by scanning electron microscopy, description of the results.

A. V. Vorontsov – analysis of X-ray data, calculation of contributions of individual hardening mechanisms.
S. Yu. Tarasov – analysis of experimental data, finalizing the text, writing conclusions, editing the article.

А. О. Панфилов – выполнение исследований микроструктуры методом оптической микроскопии, обработка и анализ результатов микроструктурных исследований, проведение механических испытаний на растяжение.
А. В. Чумаевский – выполнение исследований микроструктуры методом сканирующей электронной микроскопии, описание результатов.
А. В. Воронцов – анализ данных рентгеноструктурного анализа, расчет вкладов отдельных механизмов упрочнения.
С. Ю. Тарасов – анализ экспериментальных данных, доработка текста, формирование выводов, редактирование финальной версии статьи.

Received 02.09.2022
Revised 04.10.2022
Accepted 17.10.2022

Поступила в редакцию 02.09.2022
После доработки 04.10.2022
Принята к публикации 17.10.2022